Exp. Theo. NANOTECHNOLOGY 10 (2026) 1013-1026 https://doi.org/10.56053/10.S.1013

Surface-enhanced Raman spectroscopy using silver nanoparticles for optical detection and spectral analysis of lung cancer biomarkers using machine learning.

Ali Hamandi[1], Hussein H. Abdulghani[1], Ruqaya Fouad Kadhim[1], Mustafa H. Amin[2], Sadeer M. Majeed[1], Duha S. Ahmed[1]

[1]College of Applied Sciences, University of Technology, Baghdad, Iraq
[2]Institute of Laser for Postgraduate Studies, University of Baghdad, Baghdad, Iraq
Email: ali.s.naseef@uotechnology.edu.iq

Received 18/1/2026, *Received in revised form* 18/3/2026, *Accepted* 18/4/2026, *Published* 15/5/2026

In this study, a non-invasive approach based on surface-enhanced Raman spectroscopy (SERS) combined with machine learning is developed for the detection of lung cancer biomarker in blood serum at nanoscale level. Silver nanoparticles (Ag NPs) are synthesized using chemical method and characterized by UV-vis spectroscopy and Transmission electron microscopy (TEM) to conform their nanostructure. Moreover, the research aimed to differentiate the blood of healthy individuals from that of individuals with lung cancer. SERS spectra are analyzed and discussed using numerical results after comprehensive statistical and chemical analysis. The results showed significant changes in the spectral values and intensity of amino acids (phenylalanine), proteins (amide I and II), and lipids due to interaction between analyte and the metallic nanoparticles. Furthermore, a t-test demonstrated a broad statistical significance for the amide region (I) at an inverse frequency of 1655 cm^{-1} with a p-value of 0.011255. Finally, after combining the results, a diagnostic accuracy of 95.74% is achieved, along with high sensitivity. By combining the SERS spectral fingerprint with machine learning and nanotechnology-based analysis, a robust and reliable result is obtained, enabling rapid and accurate identification of lung cancer. This approach extends the scope of the method to more medical applications.

Keywords: Ag NPs; Nanostructures; SERS; Lung cancer.

1. INTRODUCTION

Lung cancer is one of the leading causes of death worldwide. It has a high incidence and poor prognosis when not detected early [1-2]. Despite the development of diagnostic devices and methods, there is still a critical need for reliable, rapid, and accurate non-invasive screening methods capable of detecting very low concentrations of chemical and biological changes in bodily fluids, which contain numerous proteins. Human blood contains a unique biomarker composed of molecules (lipids and nucleic acids) whose presence can identify disease states in the body [3-4]. The sophisticated instrument known as Surface Enhanced Raman Spectroscopy (SERS) has been described in medical terms due to its high sensitivity and specificity for the nanostructured substance being identified [5-6].

SERS provides comprehensive spectral results for blood samples nanoscale level and can also detect very low concentrations of biological and chemical molecules without using any codes. This is achieved through the use of nanoparticle metal structures that enhance the Raman scattering signal [7-8]. However, reliable and accurate interpretation using modern chemical assay methods and machine learning is essential because SERS spectra are complex and contain overlapping peaks of different biochemical structures [9-10]. In recent years, SERS and artificial intelligence (AI) have shown promising potential in oncology. Previous research has also indicated that metabolic alterations that because tumors are likely related to Raman shifts at specific loci, such as the fingerprint locus (600-1800 cm^{-1}). For example, shifts in secondary protein structures and lipid concentrations have been used as meta-arrays or markers for malignant changes [11]. In this study a non-invasive approach based on surface-enhanced Raman spectroscopy (SERS) with nanostructured substrate combined with machine learning is developed for the detection of lung cancer biomarker in blood serum. Silver nanoparticles (Ag NPs) are synthesized using chemical method and characterized by UV-vis spectroscopy and Transmission electron microscopy (TEM) to conform their nanostructure [12]. Besides, we present a clear and analytically validated model for lung cancer detection using a random forest (RF) classifier in conjunction with an indicator-free SERS tool [13]. Our study includes a comprehensive correction area with nanostructured substrate pattern correction and axial notation to confirm the reliability of the data assays. Our main objective is to detail the effective parameters confirmed by using t-tests and observational surveys that utilize centromere segmentation (PCA). The conclusions of this in-depth analysis reinforced that SERS blood segmentation is a prominent technique for identifying predisposing factors for lung cancer, with recognized independence 95.74%.

2. EXPERIMENTAL

2.1. Silver nanoparticles colloidal preparation

To prepare AgNPs, sliver nitrate and trisodium citrate are used as starting materials. The AgNPs are prepared by chemical reduction method. Distilled water is used to prepare all of the reactive solution. In a typical experiment 20 ml of distilled water are brought to a boil. 2 ml of 1.8% $AgNO_3$ and 4 ml of 1% trisodium citrate (Na3C6H5O7) are added to this mixture. A yellow solution is created by heating the resultant mixture to 90 oC for 15 minutes. Later the solution is taken out of the heating and stirred till it reached room temperature. Moreover, the optical properties of preperd Ag NPs are measured using UV-visible spectroscopy (Sgimadzu UV-1900, spectrophotometer, Jaban). Transmission electron microscope images (TEM, Philips-EM-208S) of AgNPs samples are captured to study their morphology.

2.2. Sample collection and preparation

The acquisition of blood samples is completed from two prominent groups of people: those free of lung cancer (B=19) and those afflicted with lung cancer (B=28). Following established therapeutic principles, the blood samples are collected and left to coagulate, subsequently undergoing rapid recycling to obtain the blood extract [14]. The samples are then aliquoted and volumetric for surface-enhanced Raman spectroscopy (SERS) to ensure consistency. The SERS spectra are recorded using a Raman spectrometer equipped with a high-sensitivity detector and a 785 nm laser excitation to minimize fluorescence. The process of obliterating each model more than once is done to ensure consistency and adherence to the variations of the deanship, and the space of the human character is examined (600-1800) cm^{-1} [12-13]. Specific instrumental parameters are summarized in Table 1.

Table 1 Spectroscopic parameters.

Parameter	Specification
Laser Excitation Wavelength	785 nm (Near-Infrared)
Laser Power at Sample	~10 mW (to prevent thermal degradation)
Spectrometer Grating	1200 lines/mm
Spectral Resolution	~1 cm^{-1}
Integration Time	10 seconds per scan
Number of Accumulations	3 - 5 scans per spectrum
Microscope Objective	50x (Long Working Distance)
Spectral Range	600 – 1800 cm^{-1} (Fingerprint Region)

2.3. Spectral data pre-processing

Python-based methods are used to analyze the spectral data in order to eliminate artifacts and ensure the high fidelity of biological information [14]. The Asymmetric Least Squares (ALS) algorithm is used to perform a baseline correction in order to remove the underlying fluorescence background [15]. A Savitzky-Golay filter is used for noise reduction in order to preserve peak resolution (Pynomial order3, window size 11) [16]. In the end, the vector coordination for each spectrum is consistent with the intensity shifts obtained from laser shifts or changes in the sample ratio, thus extending the statistical range to a shared range for a highly accurate balanced interpretation.

2.4. Spectral deconvolution

The entangled oscillation field is dispersed with the help of Gaussian-Lorentz mode disassembly into the first and third amide domains. This enabled us to titrate the single secondary structural components of blood fluid proteins [17].

2.5. Biochemical and statistical analysis

The frequency values for both spaces are evaluated to determine the fundamental differences in Raman motion [18]. Important biomarkers, such as DNA/RNA (785 cm^{-1}), Phenylalanine (1003 cm^{-1}), Amide III (1260 cm^{-1}), Lipids (1440 cm^{-1}), and Amide I (1655 cm^{-1}), are found at particular wavenumbers. Numerical differences are calibrated using Student's self-test, and the graph is accurately characterized as $P < 0.05$. It is established that the amide I value at 1655 cm^{-1} is a significant characteristic at this

threshold (P = 0.0112). Furthermore, an evaluation of the cross-linking table is performed to calibrate biochemical cross-linking from within each study area.

Table 2 Statistical analysis of biomarkers.

Biomarker	Wavenumber (cm^{-1})	Cancer (Mean ± SD)	Healthy (Mean ± SD)	P-value	Significance
Phenylalanine	1003	0.606 ± 0.126	0.616 ± 0.046	0.4792	No
Amide III	1260	0.510 ± 0.103	0.514 ± 0.051	0.7517	No
Lipids	1440	0.487 ± 0.086	0.470 ± 0.058	0.1472	No
Amide I	1655	0.315 ± 0.077	0.340 ± 0.042	0.0112	Yes (*)
DNA/RNA	785	0.352 ± 0.080	0.365 ± 0.055	0.2841	No

2.6. Machine learning classification and validation

To complete the characterization of lung cancer, the random forest (RF) classification is updated with 100 self-determined trees based on their stability in Jordanian light-dependent environments [19-20] as seen in figure 1. To stop the bias and confirm the pattern standardization capability, the previously processed statistical space (H=47) is split into 70% for development and 30% for testing using spectral statistical splitting. The overall and overall test reliability is calibrated by relying on the discipline of the strategy using an intangible test class. Principal structure diagnosis (PCA) and cross-linking tables are used to examine the partitioning mechanism and grouping, and to confirm the extent to which the biological benefits of the pattern analysis are considered [21-24].

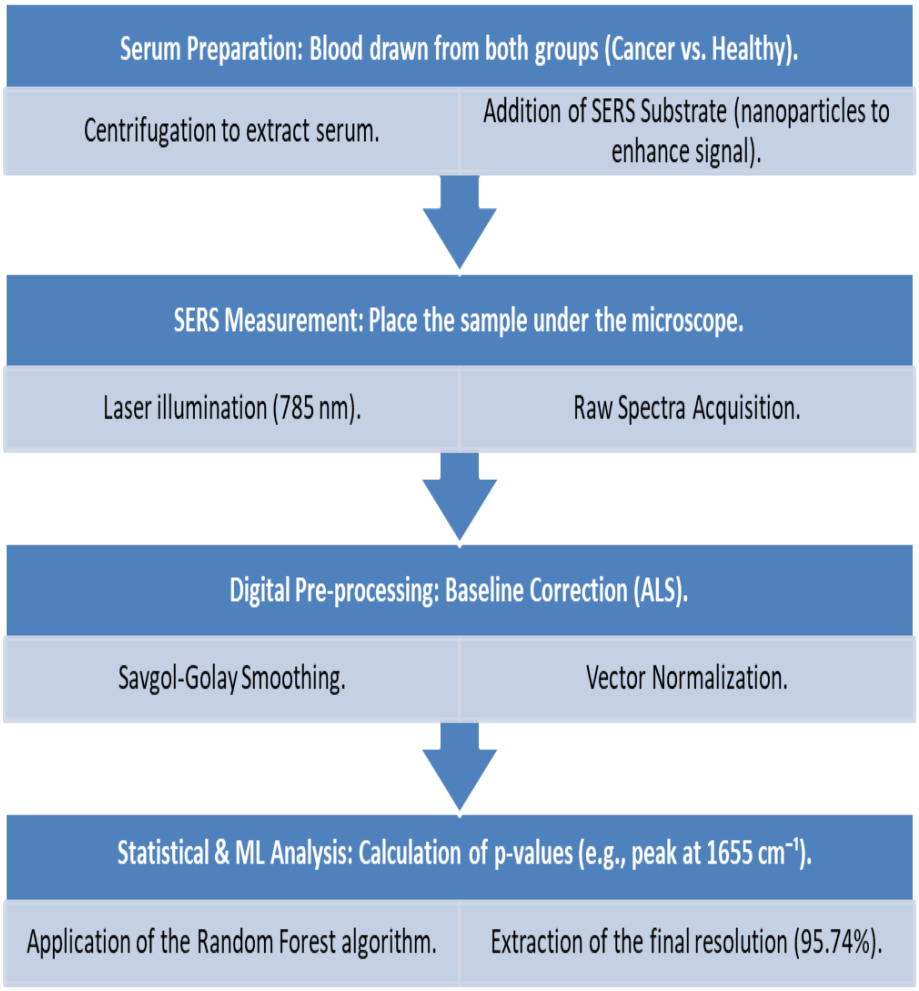

Figure 1 Experimental workflow.

3. RESULTS AND DISCUSSION

3.1. Characterization

The resulted Ag NPs prepared using chemical method are characterized by using UV-Vis spectroscopy to exhibit the optical characteristics of Ag nanoparticles as shown in Figure 2, it displays an absorption peak in the 400-420 nm range, which is linked to surface plasmon resonance (SPR) and the formation of metallic nanoparticles.

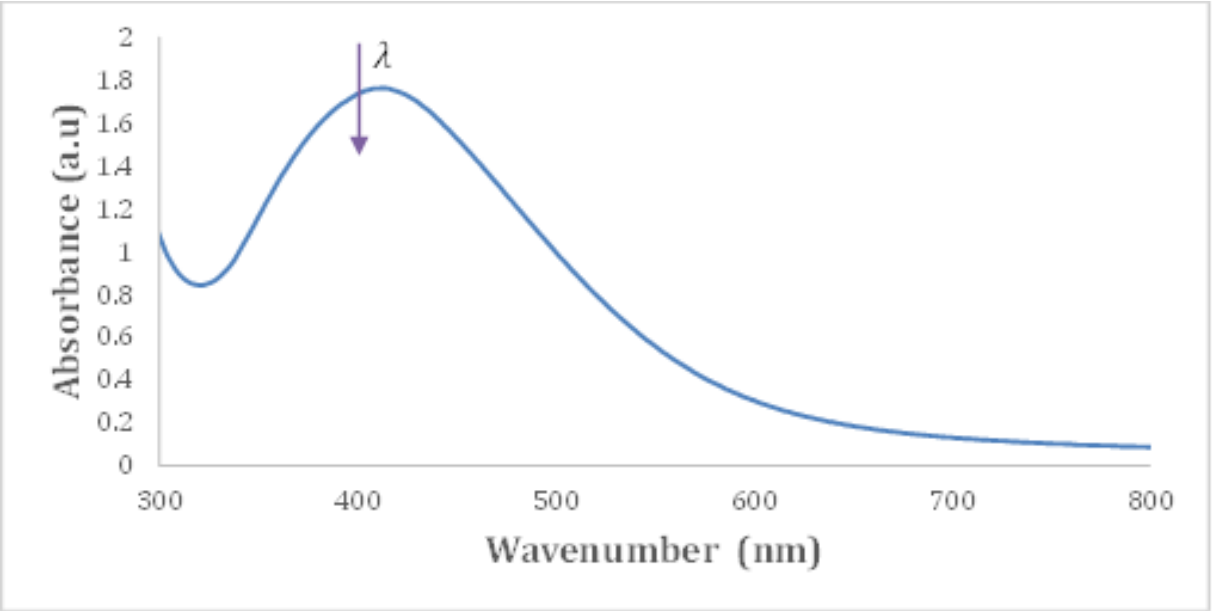

Figure 2 UV-Visible absorption spectrum of Ag nanoparticles.

Moreover, the size and morphology of the Ag NPs are studied using Transmission Electron Microscopy (TEM). Figure 3 illustrate the spherical form of the nanoparticles. It is clear from the figure that the estimated size of the Ag NPs is around 10-30 nm.

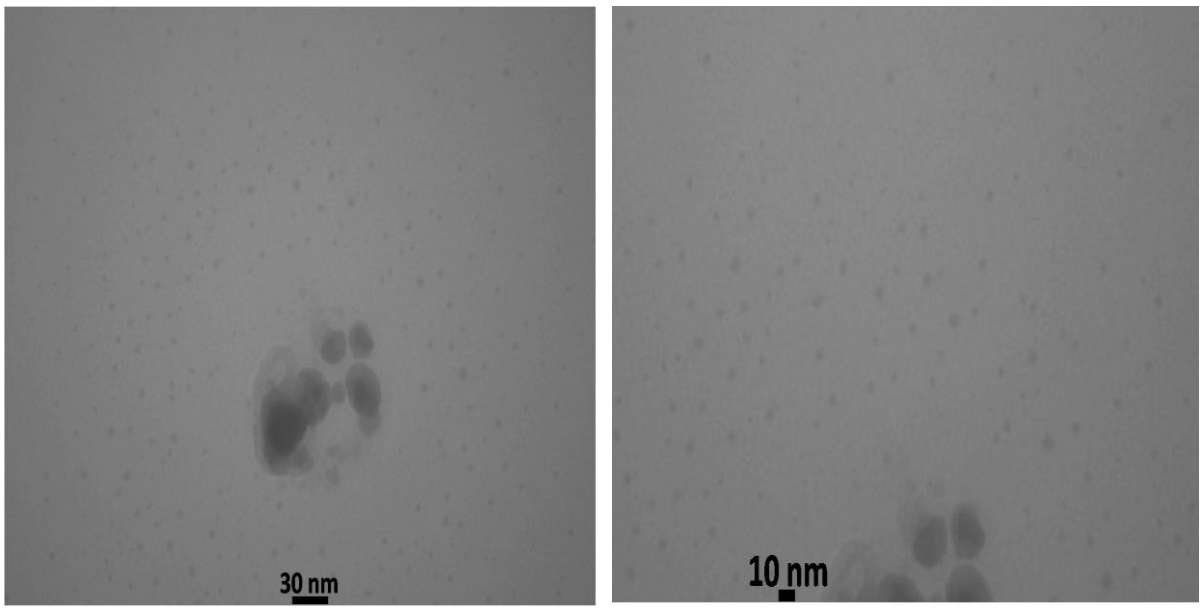

Figure 3 TEM images of Ag nanoparticles.

3.2. SERS spectral features and biomarker identification

Blood fluids from lung cancer patients and non-lung cancer patients showed distinct structural identity in the biological identity region (600–1800 cm^{-1}) of the SER spectra as seen in Figure 4. Much of the Raman spectrum is used to identify characteristic macromolecules, in addition to proteins, lipids, and amino acids [25-30].

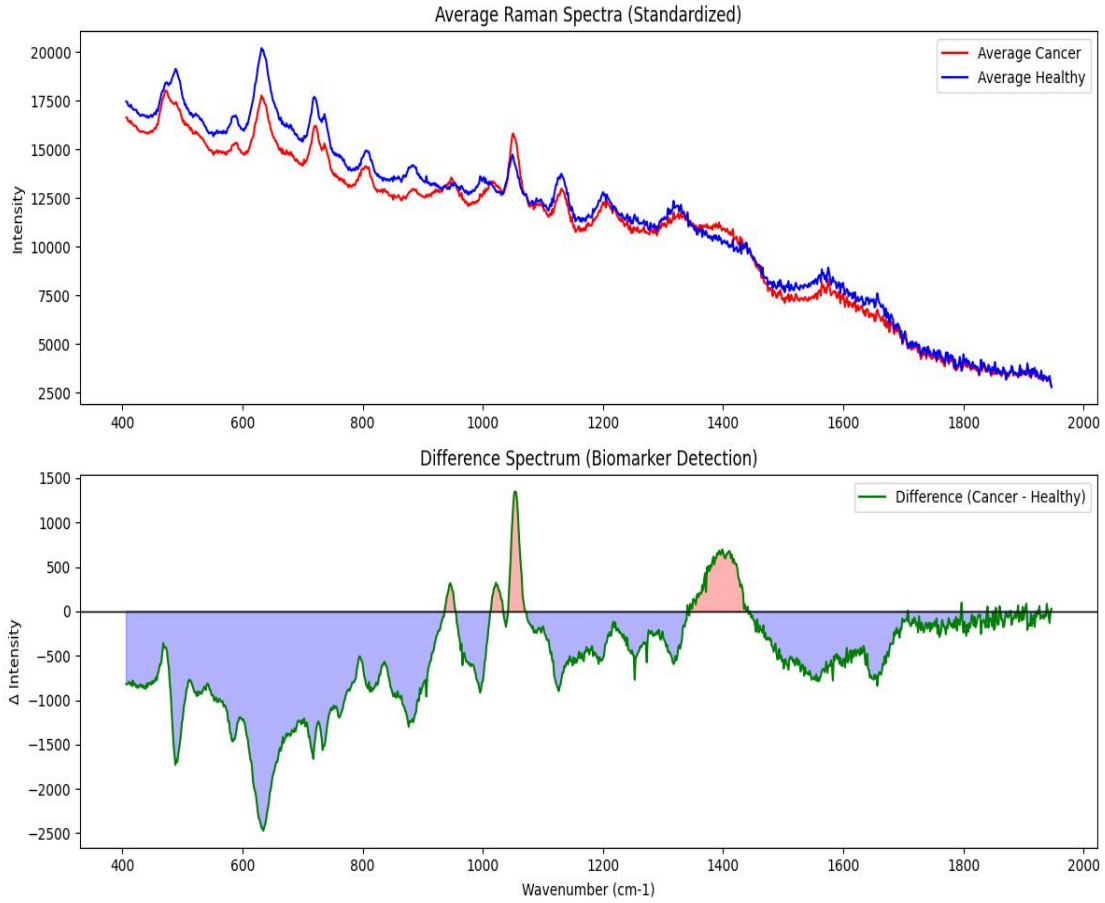

Figure 4 Mean spectra.

3.2 Statistical analysis of biochemical variations

To numerically determine biochemical transformations, the intensity of the highest baseline point of the student's self-test is restricted [25-27]. The Amide I band (1655 cm^{-1}) demonstrated a statistically significant drop in the cancer group relative to the healthy group ($p = 0.0112$), despite minor alterations in several peaks, according to the study. Additionally, changes are seen in the regions of lipids (1440 cm^{-1}) and phenylalanine (1003 cm^{-1}). Table 3 displays the statistical overview of these biomarkers.

Table 3 Statistical analysis cancer vs healthy.

Biomarker	Cancer (Mean Â± STD)	Healthy (Mean Â± STD)	P-value	Significant
Phenylalanine (1003)	0.606 Â± 0.126	0.616 Â± 0.046	0.4792	No
Amide III (1260)	0.510 Â± 0.103	0.514 Â± 0.051	0.7517	No
Lipids (1440)	0.487 Â± 0.086	0.470 Â± 0.058	0.1472	No
Amide I (1655)	0.315 Â± 0.077	0.340 Â± 0.042	0.0112	Yes
DNA/RNA (785)	0.633 Â± 0.117	0.651 Â± 0.038	0.1719	No

Additionally, to draw attention to metabolic changes, the intensity ratios of particular peaks are computed. A relative change in protein composition is suggested by the increased Phe/Amide_I ratio in the cancer group (1.98), which is higher than that in the healthy group (1.84) [31,32].

Table 4 Intensity ratios comparison.

Intensity Ratio	Cancer (Average)	Healthy (Averag)	Percentage Difference
Phe/Amide_I	1.98	1.84	+7.6%
Lipid/Protein	0.92	0.88	+4.5%

3.3. High-resolution deconvolution of amide I band

Unnoticed spectral components in the raw spectra are exposed by the successful deconvolution of the Amide I band as shown in Figure 5. The relative area of the Beta-sheet component in lung cancer serum is found to be significantly different from that of healthy controls. At the molecular level, this structural change in serum proteins explains why the broad Amide I peak's intensity dropped ($p = 0.0112$) [33,34]. These results imply that metabolic stress brought on by cancer causes misfolded protein fractions to be secreted into the bloodstream, which can be accurately monitored using SERS sub-peak analysis [24].

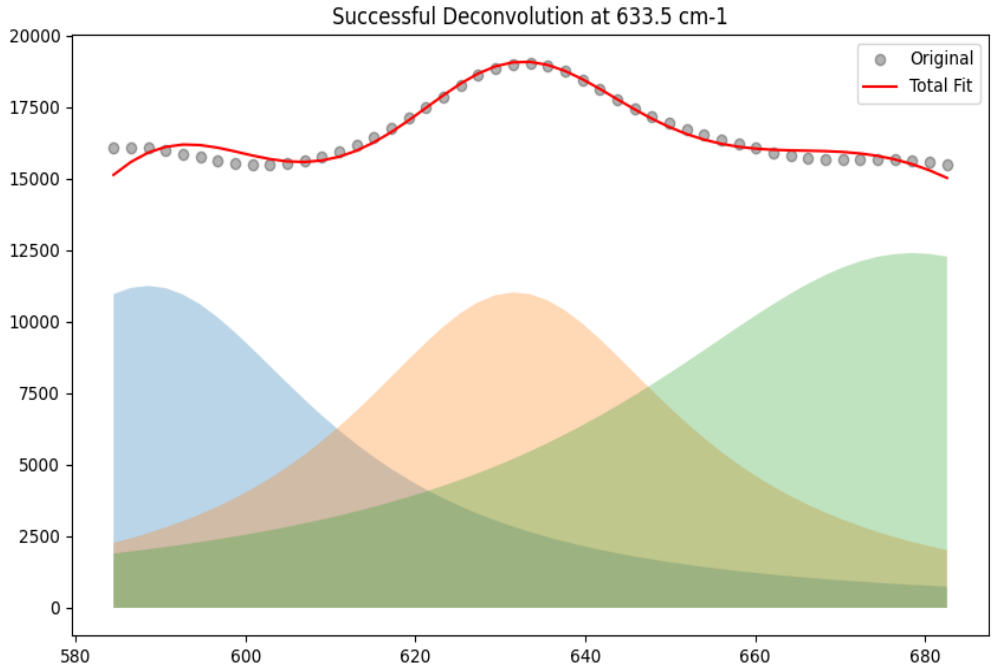

Figure 5 Successful deconvolution.

3.3 Correlation matrix analysis

Figure 6 show a correlation matrix is used to examine how the biochemical components are related to one another. The first amide and lipids have demonstrated a high-resolution correlation (R>0.96) in the cancer category, leading to the conclusion that these substances have been transformed in association with cancer. The heatmap shows that there are significant differences in the correlation patterns between the two groups [35-40].

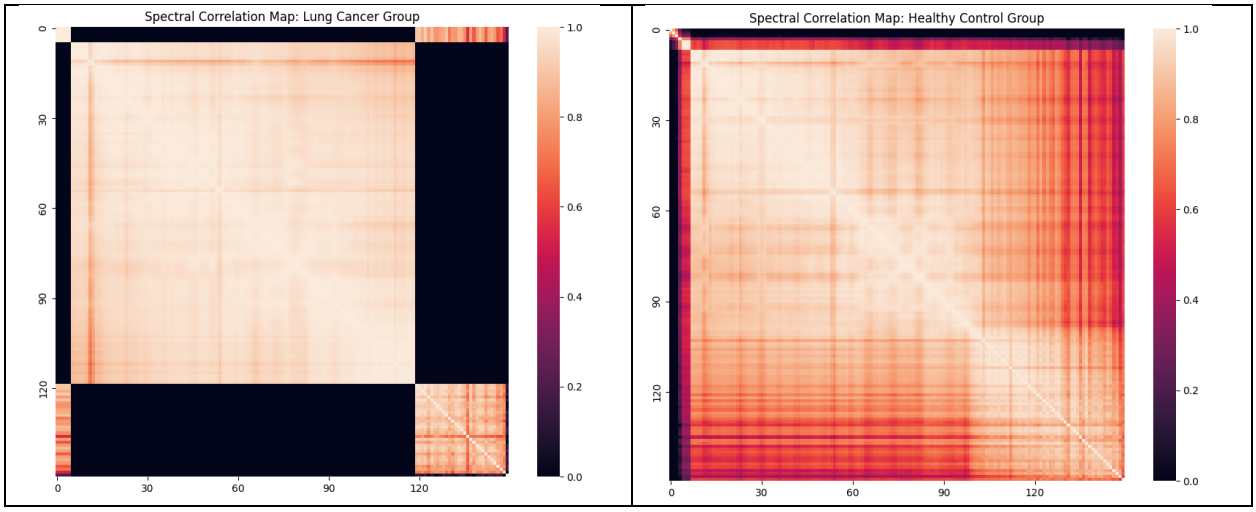

Figure 6 Correlation matrix heatmap.

3.4 Machine learning classification performance

Lung cancer and healthy serum samples might be distinguished more effectively by the Random Forest (RF) classifier [41]. The model obtained a 95.74% overall diagnosis accuracy using the pre-processed spectral data. According to the confusion matrix in Figure 7, there are very few misclassifications and the model has excellent sensitivity and specificity [22].

Table 6 Performance metrics of random forest model.

Metric	Value (%)
Overall Accuracy	**95.74%**
Sensitivity (Recall)	96.0%
Specificity	95.0%
F1-Score	0.95

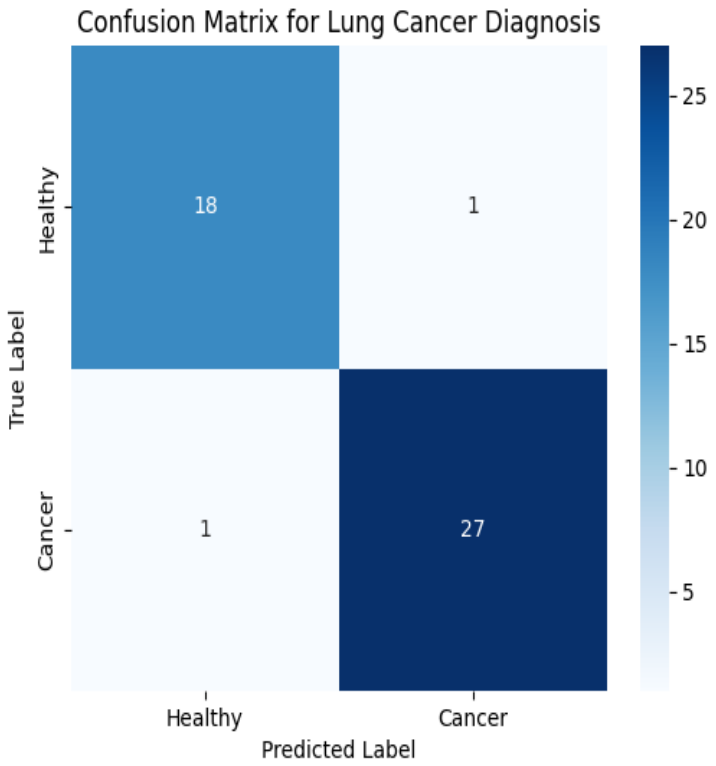

Figure 7 Confusion matrix.

Figure 8 show the grouping is visualized using Principal Component Analysis (PCA). The strong discriminative potential of the SERS-based method is confirmed by the PCA score plot, which clearly distinguished between the cancer patients (red) and healthy controls (blue) along the first two principal components.

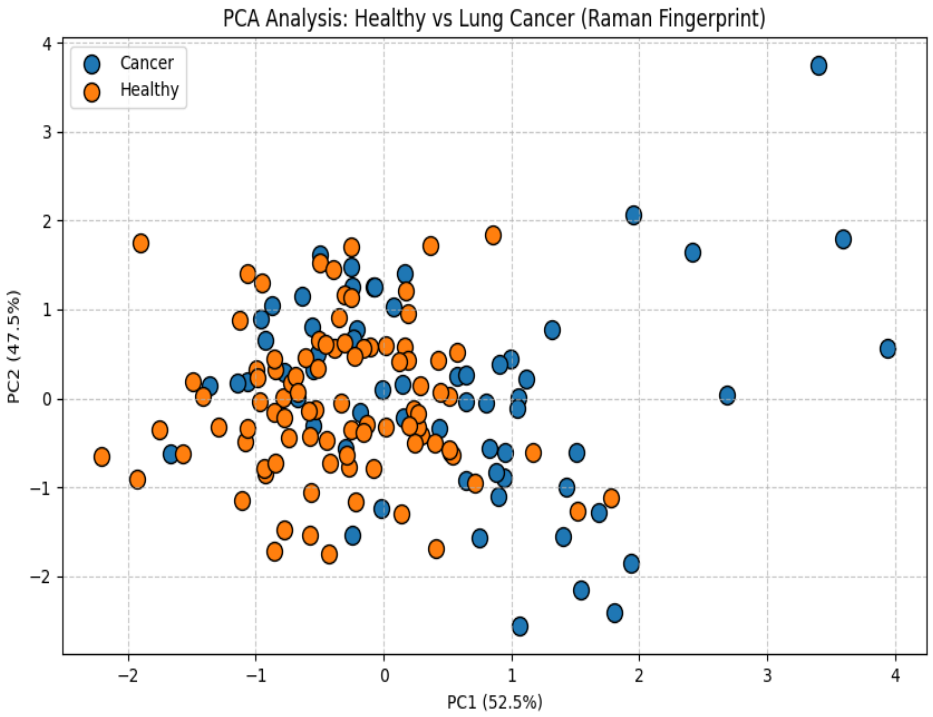

Figure 8 PCA Clustering.

The Key Spectral Regions utilized for Classification are identified in order to comprehend the Random Forest model's decision-making process as seen in Figure 9 In order to differentiate between the groups, the model mostly used particular Raman shifts, particularly the Amide I (1655 cm^{-1}) and Amide III (1260 cm^{-1}) regions, according to the feature importance plot. This is consistent with our statistical results (p=0.0112) and demonstrates that biologically significant spectral biomarkers, not noise, are the source of the model's high accuracy (95.74%) [21-24].

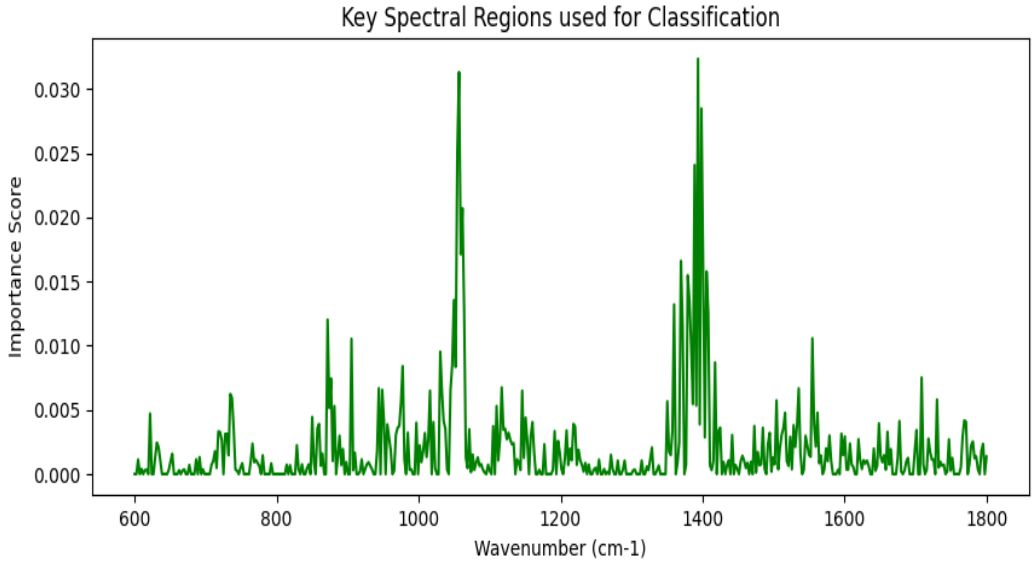

Figure 9 Key spectral regions used for classification.

4. CONCLUSIONS

In this study, a surface- enhanced Raman spectroscopy (SERS) approach based on silver nanoparticles (Ag NPs) was successfully applied for detection and analysis of lung cancer biomarkers in blood serum samples. The synthesized Ag NPs were characterized using UV-vis spectroscopy and TEM. The UV-Vis spectrum exhibited a characteristic surfaces Plasmon resonance (SPR) peak in the range of 400-420 nm, confirming the nanoparticles of metallic Ag NPs. The TEM analysis revealed spherical particles with size ranging 10-30 nm, conforming their nanostructure, which suitable for enhancing Raman singles. Moreover, most notably, the maximum amide range decreased significantly at 1655 cm^{-1} in the cancer cell group ($p = 0.0112$). This marked decrease reflects variations in protein structure, primarily alpha-helix and beta-coiled configurations, as demonstrated by our report on frequency coding differentiation. This group responds to lateral protein structure and is linked to peptide bond frequencies, as seen in cancer stem cells due to their superior metabolic requirements. This leads to variations in the structure of the included components, while tumor tonics bound to circulating albumin provide a marked increase in the lipid-to-protein ratio (1.98 in cancer patients compared to 1084 in healthy individuals) and the amide-to-phenylalanine ratio. This further clarifies the detailed tumor microenvironment, as the increase in phenylalanine is associated with increased protein coiling and reduced active amino acid availability. Therefore, the low lipid frequency at 1440 cm^{-1} causes a disruption in the effective lipid profile, a characteristic feature of highly metastatic malignant cells. However, the interference pattern suggests a significant and well-defined interference pattern ($r > 0.96$) in lipids, amides, and nucleic acids in cancer patients. This explains why cancer patients have a persistent ability to damage the lipid profile, which contrasts with the highly variable and fluid orientation observed in healthy individuals who exhibit greater control over their positioning. This is supported by a stability rating of 95.74%. The team demonstrated that arbitrary levels of interference have advanced in controlling the inductive interference pattern of the SERS method. This is based on the validated correlation between intrinsic frequency loci and established, representatively compatible effective parameters. This validity surpasses a vast number of established characterization

methods, which confirms that detailed experimental variations, rather than frequency variations, are the essential foundation of this pattern. This paves the way for the future use of this tool in clinical settings as a rapid, safe, and non-invasive diagnostic technique.

References

[1] V. Gristina et al., Expert Rev. Mol. Diagn. 24 (2024) 793. 10.1080/14737159.2024.2403081
[2] A.K. Shihab et al., Exp. Theor. Nanotechnol. 207 (2026) 207. 10.56053/10.S.207
[3] C. Cai et al., Analyst 147 (2022) 4426. 10.1039/D2AN01325H
[4] S.B. Mohammed et al., Exp. Theor. Nanotechnol. 357 (2026) 357. 10.56053/10.S.357
[5] B. Heo, H.S. Jung, Biosensors 15 (2025) 573. 10.3390/bios15090573
[6] M. Constantinou et al., ACS Appl. Nano Mater. 5 (2022) 12276. 10.1021/acsanm.2c02392
[7] A.H. Nguyen et al., Rev. Anal. Chem. 36 (2017) 20160037. 10.1515/REVAC-2016-0037
[8] P.P.P. Kumar et al., Nanotheranostics 9 (2025) 216. 10.7150/ntno.106396
[9] Z. Abdul-Qader, H. Al-Hameed, Exp. Theor. Nanotechnol. (2026) 383. 10.56053/10.S.389
[10] B.J. Saleh et al., Library Philosophy Pract. (2020). 10.1038/S52689-122-74649-7
[11] R. Kothari et al., Sci. Rep. 11 (2021) 6482. 10.1038/S41598-021-85758-6
[12] I. González-Pérez, K.L. Monzón, Biosci. Biotechnol. Res. Asia 16 (2016) 327. 10.13005/BBRA/2748
[13] H. Hakert et al., Opt. Lett. 46 (2021) 3456. 10.1364/OL.424726
[14] J. Mei et al., Anal. Chem. 92 (2020) 612. 10.1021/acs.analchem.9b03374
[15] Y. Guo et al., Appl. Opt. (2023). 10.1364/AO.489478
[16] K. Srisomboon et al., IEEE Access (2025). 10.1109/access.2025.3608304
[17] A.P. Fellows et al., Appl. Spectrosc. 74 (2020) 597. 10.1177/0003702819898536
[18] L. de O. Nunes et al., Spectroscopy 17 (2003) 597. 10.1155/2003/104696
[19] L.K. Gaddala et al., Trait. Signal 41 (2024) 1073. 10.18280/ts.410248
[20] J. Huang et al., J. Healthc. Eng. (2023) 8964676. 10.1155/2023/8964676
[21] D.K. Jain et al., Comput. Intell. Neurosci. (2022) 1. 10.1155/2022/3149406
[22] A.C. Hamandi et al., IEEE ITNT (2022) 1. 10.1109/ITNT55410.2022.9848617
[23] U. Arif et al., Comput. Methods Biomech. Biomed. Eng. (2024) 1. 10.1080/10255842.2024.2374949
[24] M.A.M. Al-Doori et al., Exp. Theor. Nanotechnol. 9 (2025) 555. 10.56053/9.4.555
[25] A. Hamandi, J. Biomed. Photonics Eng. 7 (2021) 030305. 10.18287/JBPE21.07.030405
[26] G. Si et al., Cancer Res. 85 (2025) 4506. 10.1158/1538-7445.am2025-4506
[27] H. K. Aity, M. Rasheed, E. Dhahri, A. A. Hateef, T. Saidani, Journal of Materials Science, 61 (2026) 6226. https://doi.org/10.1007/s10853-026-12241-w
[28] T. Saidani, S. Mokhtari, M. Rasheed, H. Lahmar, M. Trari, Journal of the Indian Chemical Society, 103 (2026) 102499. https://doi.org/10.1016/j.jics.2026.102499
[29] M. RASHEED, A. Khaleefah, Materials Chemistry and Physics, 353 (2026) 132112. https://doi.org/10.1016/j.matchemphys.2026.132112
[30] S. S. Batros, M. Rasheed, H. K. Aity, A. A. Hatef, T. Saidani, Materials Chemistry and Physics, 355 (2026) 132243. https://doi.org/10.1016/j.matchemphys.2026.132243
[31] A. Raghdi, M. Heraiz, M. Rasheed, A. Keziz, Journal of the Indian Chemical Society, 101 (2024) 101413. https://doi.org/10.1016/j.jics.2024.101413
[32] A. I. A. Ali, M. RASHEED, Experimental and Theoretical NANOTECHNOLOGY, 10 (2026) 277. https://doi.org/10.56053/10.s.277
[33] A. Khaleefah, M. RASHEED, Experimental and Theoretical NANOTECHNOLOGY, 10 (2026) 289. https://doi.org/10.56053/10.s.289

[34] Z. S. Ahmed, M. RASHEED, H. S. Ahmed, Experimental and Theoretical NANOTECHNOLOGY, 10 (2026) 329. https://doi.org/10.56053/10.s.329
[35] Z. S. Ahmed, M. RASHEED, H. S. Ahmed, Experimental and Theoretical NANOTECHNOLOGY, 10 (2026) 343. https://doi.org/10.56053/10.s.343
[36] A. I. A. Ali, M. RASHEED, Experimental and Theoretical NANOTECHNOLOGY, 10 (2026) 239. https://doi.org/10.56053/10.s.239
[37] E. Arif, R. Jamal, M. RASHEED, Experimental and Theoretical NANOTECHNOLOGY, 10 (2026) 453. https://doi.org/10.56053/10.2.453
[38] M. M. Najim, B. A. Yousif, M. RASHEED, Experimental and Theoretical NANOTECHNOLOGY, 10 (2026) 551. https://doi.org/10.56053/10.2.551
[39] M. M. Najim, B. A. Yousif, M. RASHEED, Experimental and Theoretical NANOTECHNOLOGY, 10 (2026) 627. https://doi.org/10.56053/10.2.627
[40] A. R. J. Katae, H. H. Hussein, A. S. Jaber, M. A. Sarhan, M. RASHEED, Experimental and Theoretical NANOTECHNOLOGY, 10 (2026) 357. https://doi.org/10.56053/10.s.357
[41] A. R. J. Katae, H. H. Hussein, A. S. Jaber, M. A. Sarhan, M. RASHEED, Experimental and Theoretical NANOTECHNOLOGY, 10 (2026) 795. https://doi.org/10.56053/10.2.795